Available online at www.sciencedirect.com
ScienceDirect
Chemical Geology 249 (2008) 237–249
CHEMICAL GEOLOGY INCLUDING ISOTOPE GEOSCIENCE
www.elsevier.com/locate/chemgeo

EXAFS analysis of cadmium(II) adsorption to kaolinite

Igor F. Vasconcelos [a,*], Elizabeth A. Haack [b], Patricia A. Maurice [b], Bruce A. Bunker [a]

[a] Department of Physics, University of Notre Dame, Notre Dame, IN, 46556, USA
[b] Department of Civil Engineering and Geological Sciences, University of Notre Dame, Notre Dame, IN, 46556, USA

Received 3 October 2007; received in revised form 28 December 2007; accepted 7 January 2008

Editor: J. Fein

Abstract

The local molecular structure of Cd sorbed to kaolinite was examined with X-ray absorption fine structure spectroscopy (XAFS) over a range of pH and initial Cd solution concentrations, ($[Cd_{aq}]_{in}$). Quantitative analysis of kaolinite samples with $[Cd_{aq}]_{in}$ of 100 μM and pH 7, shows a single hydration sphere around Cd, consistent with an outer-sphere adsorption complex. At pH 9, a Cd–M coordination (where M stands for Si or Al) at second shell distance indicates the formation of inner-sphere adsorption complex(es) on edge sites. Although adsorption to Al edge sites is probably preferred, the similarity in atomic numbers between Al and Si and the small difference in bond lengths prevents us from distinguishing complexation to Si- versus Al-edge sites based on the XAFS data. The possibility of precipitation of Cd solid phases was ruled out due to similar local environment around Cd in samples prepared under air (where carbonate species would be present) and N_2 atmospheres, and the absence of a Cd–Cd coordination characterizing a Cd-bearing solid phase. Finally, analysis of kaolinite samples with $[Cd_{aq}]_{in}$ of 3 μM, 10 μM, and 100 μM at pH 9 shows a consistent change in Cd–M distance and Debye–Waller factor as a function of $[Cd_{aq}]_{in}$, suggesting a change in the type of inner-sphere complex being formed as a function of loading. Whether this means that there is a change in the relative importance of Al versus Si edge sites with loading, or whether adsorption of Cd to edge sites alters binding to other nearby sites, or some other factor, has not been determined at this time.

Keywords: Kaolinite; Adsorption; Cadmium; XAFS

1. Introduction

Development of a molecular-based understanding of metal binding to mineral surfaces is crucial for accurate predictive modeling of metal fate, transport, and retardation. Clay minerals can play an important role in metal transport in soil and aquifer environments and have been the focus of many studies for contaminant remediation (Papini et al., 2001; Kugler et al., 2002; Yavuz et al., 2003).

Kaolinite is a 1:1 non-swelling clay that is widely distributed. Kaolinite can be immobile, or it can be a mobile colloid (Kaplan et al., 1995). When associated with stationary kaolinite particles, a metal's mobility would decrease. In contrast, association with colloid-sized kaolinite may increase the mobility of the metal. Individual kaolinite layers are composed of one gibbsite-like sheet of Al octahedra (in which two of the three octahedral sites are filled) bonded through shared oxygen atoms to one sheet of Si tetrahedra. Layers are held together by hydrogen bonding between oxygen atoms of the siloxane sheet and hydroxyl groups associated with the gibbsite sheet. Because of this hydrogen bonding, and because there is little isomorphic substitution for Al in the octahedral positions and for Si in the tetrahedral positions, the permanent charge and thus the exchange capacity of kaolinite is minimal in comparison to the swelling clays (Ferris and Jepson, 1975; Sposito,1984; Chorover and Sposito, 1995).

Kaolinite clay has two general classes of sites with the potential to interact with dissolved metal cations: (1) sites on the basal (001) faces of the clay; and (2) sites at the particle edge

* Corresponding author. Present address: Universidade Federal do Ceará, Fortaleza, Brazil. Tel.: +55 85 33669362; fax: +55 85 33669969.
E-mail address: ifvasco@ufc.br (I.F. Vasconcelos).

0009-2541/$ - see front matter © 2008 Elsevier B.V. All rights reserved.
doi:10.1016/j.chemgeo.2008.01.001

(Sposito, 1990; Brady et al., 1996). Functional groups associated with the siloxane basal face are Si–O–Si sites, which are generally considered to be unreactive (Sposito, 1984). Limited isomorphic substitution creates sites of permanent (i.e., not pH dependent) negative charge that are relatively diffuse. Cations are exchanged at such sites and have been shown, through molecular modeling, to sit above ditrigonal cavities associated with the siloxane basal surface (Vasconcelos et al., 2007). On the gibbsite face, sites where a hydroxide group is bridged between two Al atoms (Al–OH–Al) may be reactive, although modeled surface charge density for kaolinite has indicated that edge sites associated with the gibbsite sheet show a much stronger Lewis base behavior as compared to sites on the gibbsite basal face (Brady et al., 1996). At the particle edge, three types of sites arise from the kaolinite structure and are described in some detail by O'Day et al. (1994). These are: (1) sites where an OH group is bonded to a single Al atom (Al–OH); (2) sites where the surface oxygen atom bridges Al and Si atoms (Al–O–Si); and (3) sites where a surface oxygen atom is bonded to one Si atom (Si–O). At the particle edge, Al–OH and Si–O are regarded as the most reactive sites for adsorption of ions (Sposito, 1984) while bridging Al–O–Si are not usually considered in such reactions (O'Day et al., 1994).

As with other metal-mineral interactions (Brown and Parks, 2001; Manceau et al., 2002; McNear et al., 2005; Brown et al., 2006) interactions between metals and the kaolinite surface are being explored at the molecular scale by combining traditional geochemical approaches with synchrotron-based techniques such as X-ray absorption fine structure spectroscopy (XAFS). Results to date indicate that the sorption behavior of a metal to kaolinite is dependent on a number of experimental parameters including the identity of the metal itself, pH, ionic strength, aging, and metal:solid ratio. Note that sorption is used in this manuscript to refer generally to accumulation of the metal at the kaolinite surface, when the mechanism(s) of accumulation is not known or when more than one mechanism is involved. When metal cations sorb to kaolinite, absorption of the cation within the structure of the clay is not expected due to hydrogen bonding between subsequent layers, but adsorption (inner or outer-sphere) and precipitation (three-dimensional accumulation) may occur.

Molecular-level analysis of metal binding to kaolinite has been carried out for Sr(II), and various divalent transition metals. Irrespective of pH and aging, Sr(II) is adsorbed to kaolinite as a hydrated outer-sphere complex at negatively charged (basal and edge) sites (Parkman et al., 1998; Chen and Hayes, 1999; Sahai et al., 2000). In contrast, transition metals such as Cu(II), Co(II), and Ni(II) show more complex behavior. At high ionic strength (0.1 M $NaNO_3$), the hydrated Cu(II) ion is adsorbed as an outer-sphere complex at low pH values (2.5–4.5) but occurs as both mononuclear and binuclear inner-sphere complexes at the particle edge at higher pH values (Peacock and Sherman, 2005). Under similar conditions (pH values ~7–8, 0.01–0.1 M $NaNO_3$), Co(II) is adsorbed as inner-sphere bidentate complexes at the particle edge (O'Day et al., 1994). The exact complex depends on surface coverage, and multinuclear complexes were observed at surface coverages below monolayer. With aging, precipitation of a hydrocalcite-like solid, containing both Co and Al, also occurs due to dissolution of the kaolinite (Thompson et al., 2000). Eick et al. (2001) showed that Ni(II) sorption occurred in two stages: rapid surface adsorption was followed by slower precipitation of a Ni–Al layered double hydroxide (LDH). Further, through desorption experiments, these authors also showed that there were strong kinetic influences on precipitate growth and structure.

Sorption complexes of Cd(II) with kaolinite have not been examined at the molecular level, despite Cd being a widespread priority contaminant that is toxic to ecosystem and human health (EPA, 2002). Bulk batch adsorption experimental results suggest that Cd can adsorb both as an outer-sphere complex at negatively charged basal sites and as an inner-sphere complex at the edges of the clay (Schindler et al., 1987; Spark et al., 1995; Angove et al., 1997). Specifically, the extent of Cd sorption over the pH range of approximately 4–7 is ionic strength dependent. At solution ionic strength of 0.05 M (KNO_3), Cd(II) sorption showed low proton stoichiometry (0.2), consistent with outer-sphere adsorption at exchange sites on the Si basal plane. However, at more alkaline pH values, Cd(II) is sorbed in a manner not dependent on ionic strength. It has been suggested that Cd(II) forms a bidentate inner-sphere complex with sites on the kaolinite edge at these more alkaline pH values (Schindler et al., 1987; Angove et al., 1997), and that sorption likely occurs at aluminol sites. The objective of this study was thus to characterize the molecular-scale structure of surface complex (es) formed when Cd(II) is sorbed at the kaolinite–water interface. Our work focused on the local binding environment of Cd(II) sorbed to kaolinite at a range of different pH and initial Cd concentration conditions and over a relatively short reaction period (i.e. in the absence of significant kaolinite dissolution).

2. Materials and methods

2.1. Sorption experiments

Cadmium sorption to kaolinite was examined as a function of pH at constant initial Cd(II) concentration (sorption edge), and as a function of Cd(II) concentration at constant pH (sorption isotherm). Both experimental series were run with a background electrolyte of 0.1 M $NaClO_4$. pH values of 4.5–9.0 and a $[Cd_{aq}]_{in}$ of 100 μM were used in the sorption edge experiment. This Cd concentration was chosen to maximize the extent of Cd(II) sorption to kaolinite, and thus optimize the signal to noise ratio for the XAFS measurements, while maintaining solutions that were undersaturated with respect to $Cd(OH)_2$. $[Cd_{aq}]_{in}$ were between 9–100 μM in the sorption isotherm experiment and the initial pH in each sample was 9. Final pH values in the sorption isotherm experiment was 8.6.

Prior to sample preparation, the aqueous phase speciation of Cd was predicted using the thermodynamic model PhreeqC, version 2 (Parkhurst and Appelo, 1999). Under the experimental conditions of both sets of experiments (pH and $[Cd_{aq}]_{in}$) and ambient conditions, all parent solutions (i.e initial conditions, modeled in the absence of clay) were

predicted to be supersaturated with respect to otavite ($CdCO_3$). Thus, EXAFS analysis was carefully checked for any evidence of potential precipitation. As discussed below, there was no evidence of precipitation under the conditions of our sorption experiments. As there is sorption of Cd in the presence of clay, speciation of the parent solution provides a conservative means of predicting the potential for precipitation in the experimental solutions. Hepinstall et al. (2005) did not detect any loss of Cd in their control samples under conditions predicted to be supersaturated with respect to otavite. Further, a white precipitate observed (Papelis et al., 1995) in sorption experiments of Cd(II) to alumina at elevated Cd(II) concentrations was determined by EXAFS not to be otavite but to be $Cd(OH)_2$ or Cd hydroxycarbonate. Both these results suggest that precipitation of otavite will not contribute to loss of Cd from solution under the experimental conditions of this work. However, in this study, loss of dissolved-phase Cd due to precipitation was assessed by performing parallel adsorption edge experiments under both ambient conditions (presence of CO_2), as described above, and under N_2 atmosphere (anaerobic chamber: 95% high purity N_2, 5% H_2). All solutions used were purged with N_2 prior to being placed in the chamber. Subsequently, all supplies, solutions and clay samples (pre-weighed into acid-washed vessels) used in the preparation of sorption samples were further purged of O_2 and CO_2 overnight in the anaerobic chamber prior to the reaction period.

The clay used was the well ordered source clay KGa-1b (Clay Minerals Society Source Clay, Purdue University, IN). The clay was washed following Sutheimer et al. (1999), which includes rinsing repeatedly in 1 M NaCl adjusted to pH 3 with HCl until the pH of the supernatant is 3.0, then repeated washing in deionized water until the conductivity of the supernatant decreases to 300 mS/cm and the pH is higher than 5.5 (Sutheimer et al., 1999). KGa-1b clay pre-cleaned in this manner has a point of zero net proton charge (pH_{znpc}) of 5.1 ±0.2 (Sutheimer et al., 1999), BET surface area of 12.6 m^2/g (Sutheimer et al., 1999), and mean particle diameter of 586 nm (Sutheimer et al., 1999).

Duplicate samples and controls (no clay or no Cd) were prepared in acid-washed polypropylene bottles to a final volume of 200 mL, clay concentration of 2.06 g/L, and 0.1 M $NaClO_4$. Cd was added as $Cd(NO_3)_2$ (Fisher ICP standard solutions) and ultrapure water (Milli-Q®) was used throughout. The pH was adjusted in each sample using NaOH or HNO_3, recording the amount of acid or base added and not exceeding 1% of the initial volume. Samples were prepared under ambient conditions with the exception of a subset of samples in the adsorption edge experiment, described above. While equilibrating over a 4 hour period (Hepinstall et al., 2005), the samples were shaken gently at 100 rpm on a shaker table at room temperature (22±2 °C). Following the reaction period, samples were centrifuged for 20 min at 7500 rpm. The supernatants were removed and filtered through 0.2 μM hydrophobic filters (Millipore PTFE filters), discarding the first milliliter of filtrate, diluted as necessary, and acidified prior to analysis for dissolved Cd concentrations. The Cd-sorbed kaolinite pastes were kept at 4 °C until analysis by XAFS within 4 days.

2.2. Analysis of dissolved Cd(II) concentrations

Dissolved Cd concentrations ($[Cd]_{aq}$) in samples and controls were quantified by Inductively Coupled Plasma Optical Emission Spectroscopy (ICP-OES; Optima 3000 XL, Perkin Elmer) using an internal standard (Y) and matrix matched standards. The amount of Cd sorbed was calculated as the difference between the initial concentration and that measured in the sample supernatants.

2.3. XAFS experiments and data analysis

Table 1 summarizes samples used for XAFS measurements. Sample holders for Cd-sorbed kaolinite pastes and the aqueous

Table 1
List of samples for XAFS analysis

Sample	$[Cd_{aq}]_{in}$ (μM) [a]	$[Cd_{aq}]_{eq}$ (μM) [b]	$[Cd_{adsorbed}]_{eq}$ (μmol/m^2)	pH_{eq} [2]	atm	% Cd adsorbed [b]	Edge step
a	Cd(II) perchlorate standard solution measured in transmission						
b	100	96.1	0.14	7.2	Air	2.9	7%
c	100	85.0	0.32	8.2	Air	8.7	23%
d	100	59.0	1.43	9.1	Air	37.8	62%
e	100	73.0	1.10	8.9	N_2	26.8	65%
f	1000	n.a. [c]	n.a. [c]	8.7	Air	n.a. [c]	0.3 [d]
g	10	3.8	0.26	8.8	Air	66.0	29% [e]
h	3	0.6	0.10	8.8	Air	85.0	17% [e]

All samples were measured in fluorescence mode unless otherwise noted. Edge steps are obtained by XAFS.

[a] Initial concentrations were within 2% of the values shown.

[b] Reported values of $[Cd_{aq}]_{eq}$, $[Cd_{sorbed}]_{eq}$, pH_{eq}, and % Cd sorbed are based on duplicate samples. Relative standard deviation of pH_{eq} values was <1%. Relative standard deviations of $[Cd_{maq}]_{eq}$, $[Cd_{sorbed}]_{eq}$, and % Cd sorbed values were greatest at circumneutral pH (7 and 8) and at low $[Cd_{aq}]_{in}$, but did not exceeded 20%.

[c] Precipitation occurred in both Cd control (no kaolinite) and Cd–kaolinite samples at elevated initial Cd concentration (1000 μM).

[d] Measured in transmission.

[e] Measured with a Pd 4 filter.

standard ($Cd(ClO_4)_2$) were Plexiglas cells with windows sealed with Kapton tape. Crystalline standards for XAFS measurements were prepared by spreading commercial powders on Kapton tape and folding it several times until the desired thickness was achieved, i.e. the proper edge-step for EXAFS analysis was achieved. The aqueous standard for Cd(II) was 0.1 M $Cd(NO_3)_2$ in 0.1 M $NaClO_4$. The pH of this solution was adjusted to 3.0. XAFS experiments were performed at the Materials Research Collaborative Access Team (MR-CAT) sector 10-ID at the Advanced Photon Source (APS).

Cd K-edge (26711 eV) XAFS was measured in transmission mode for standard compounds and in fluorescence mode for clay samples. The undulator was tapered and held at fixed gap, while the X-ray energy was scanned by using the Si(111) reflection of the double-crystal monochromator. Higher harmonics were rejected by using a Pt mirror. The beam was defined by 1 mm × 1 mm slits. Linearity checks (Kemner et al., 1994) were performed for all the samples and indicated less than 0.2% non-linearity at 50% decrease in beam intensity. Incident beam intensity was monitored by an ion chamber filled with nitrogen (about 1% absorption) and varied less than 20% over the scan energy range. Energy calibration was monitored during data collection by acquiring reference Cd foil spectra simultaneously.

Transmission XAFS spectra were collected by an ion chamber filled with nitrogen and argon in roughly equal amount while fluorescence spectra were collected using a Stern-Heald detector filled with Kr. A total of 20 to 120 3-minute quick scans were collected, depending on the Cd concentration on each sample, to obtain a signal-to-noise ratio sufficiently high for EXAFS analysis. A Pd 4-absorption-length filter was used in some measurements to optimize the signal-to-noise ratio. A total of 20 3-minute quickscans were collected for each standard compound.

The software used in the data analysis include FEFF8 (Ankudinov et al., 1998) for calculation of theoretical EXAFS and AUTOBK (Newville et al., 1993), IFEFFIT (Newville, 2001) and their graphical interfaces ATHENA and ARTEMIS (Ravel and Newville, 2005) for background subtraction and fitting. Data analysis was carried out in the standard way described in Koningsberger and Prins (1988). The several scans were aligned by the reference spectra and merged in energy space. Pre-edge background was removed and spectra normalizedto a step height of 1. Edge energies, E_0, were chosen at the inflection points of the absorption edges. Post-edge background was removed to isolate the EXAFS oscillations in energy space ($\chi(E)$ data) that were then converted to wavenumber space ($\chi(k)$ data) where thephotoelectron wavenumber is given by $k = \sqrt{2m(E-E_0)^2/\hbar^2}$, with $E = \hbar\omega$ being the energy of the incident photon. The $\chi(k)$ data is described by the EXAFS equation:

$$\chi(k) = \sum_j \frac{S_0^2 N_j F_j(k)}{kR_j^2} e^{-2k^2\sigma^2} e^{2R_j/\lambda(k)} \sin\left[2kR_j + \delta_j(k)\right] \qquad (1)$$

where the sum is taken over the possible scattering paths the ejected photoelectron traverses before it comes back to the absorber atom. Here, $F_j(k)$, $\delta_j(k)$, and $\lambda(k)$ are the effective scattering amplitude and phase shift and mean free path of the scattering photoelectron, S_0^2 is the passive electrons reduction factor, N is the multiplicity of the path, R_j is the half-length of the path, and σ_j is the relative mean-square displacement of length of the path (Debye–Waller factor).

Effective scattering amplitudes $F_j(k)$ and phase shifts $\delta_j(k)$ are calculated by FEFF for a cluster of atoms based on their coordinates. These values are used in a least-squares fitting routine to obtain the values of the structural parameters N_j, R_j, and σ_j that best fit the data. The value of S_0^2 is calibrated by measuring and fitting standard compounds of known structure. For the present work, we used a crystalline CdO standard (Acros Organics; measurement not shown) to find the empirical S_0^2 value of 1.03 ± 0.09 we used in all fits. Other crystalline standards used were $Cd(OH)_2$ and $CdCO_3$ (Sigma-Aldrich Co.).

Quantitative analysis of the EXAFS for the sorption samples was restricted to the range $R = 1.2$ Å to $R = 3.2$ Å. This range was appropriate due to increased signal-to-noise ratio with decreasing pH (edge step in Table 1) and because features beyond $R = 3.0$ Å had very low amplitude in all measurements. Fits to all samples and standards were performed using simultaneous k-weighting of 1, 2, and 3 to decrease the possibility that correlations between fitting parameters compensate for a misfit in a particular k-weighting. All fits initially included a first shell of oxygens and a second shell was included subsequently in the model when it eliminated a clear misfit and significantly decreased the χ_ν^2 and $\mathcal{R}$-factor values (see below). The good quality of the fits in this first shell region can potentially dominate the calculation of goodness-of-fit parameters and bias the analysis. To better assess the quality of the fits beyond the first shell region, the contribution to the goodness-of-fit parameters in the range $R = 2.2$ Å to $R = 3.2$ Å was isolated by leaving out the range where the oxygen paths contribute the most. Typically, values of the $\mathcal{R}$-factor for the entire fitting range were about 0.001 or less.

The quality of a fit is determined by the EXAFS reliability factor $\mathcal{R}$, which measures the relative misfit with respect to the data, and χ_ν^2 which takes into account the uncertainty level in the data as well as the number of free parameters allowed to vary in a fit (N_{idp}), and the number of variables used in the model (N_{var}), where $\nu = N_{\mathrm{idp}} - N_{\mathrm{var}}$ (Newville, 2001). In an ideal situation, a good fit has $\chi_\nu^2 = 1$ (in practice, the value of χ_ν^2 is typically a few orders of magnitude larger than 1) with standard deviation of $\sqrt{2/\nu}$. A fit is considered better than another when the reduction of χ_ν^2 is of the order of $2\sqrt{2/\nu}$, or two standard deviations. The value of χ_ν^2 is used to compare two fits to the same data while the $\mathcal{R}$-factor determines how well the theoretical fit follows the experimental data. Taking the particular characteristics of the data analyzed in this work (with typical ν values of 2), a fit is considered significantly better than another when there is a reduction of χ_ν^2 approximately by a factor of 2, accompanied by a smaller value of $\mathcal{R}$.

The average uncertainty in the data, ε, is estimated by IFEFFIT as the root-mean-square average of the EXAFS signal at large values of R between 15 and 25 Å (Newville, 2001),

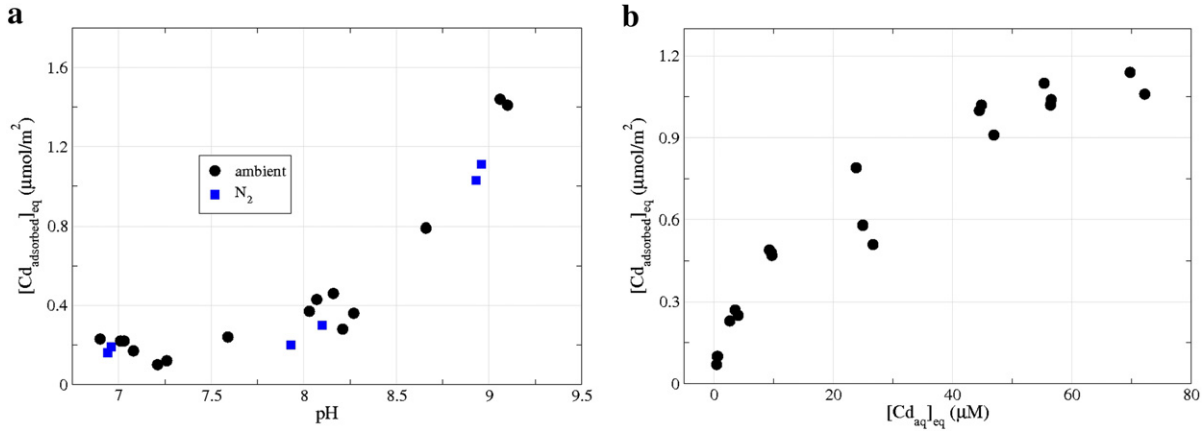

Fig. 1. Adsorption edge (a) and adsorption isotherm (b) for Cd(II) to kaolinite clay. The pH-dependent adsorption of Cd(II) to kaolinite (a) was measured in parallel under N_2 (open squares) and ambient conditions (filled squares). The adsorption isotherm (b) was measured at pH 9. Values plotted are for duplicate samples.

where no structure is expected to be found and the signal is dominated by random noise. The typical value of ε found for all the fits presented in this work is ~0.0001. This value is likely too small, as this approach usually underestimates the in-band noise. This explains the seemingly large values of χ^2_ν found throughout this work. As the main purpose of χ^2_ν is to compare different fits to the same data, the overestimated character of its values is irrelevant.

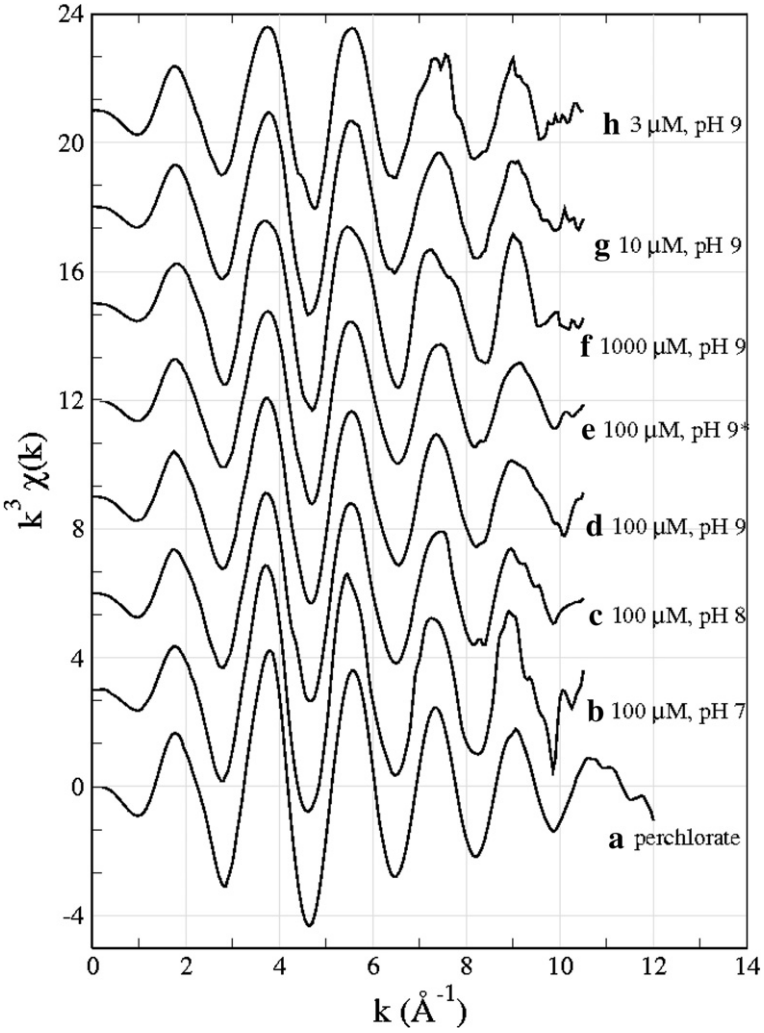

Fig. 2. k^3-weighted $\chi(k)$ data.

3. Results and discussion

3.1. Cd adsorption edge

As expected from previous observations (Hepinstall et al., 2005), the extent of Cd sorption to kaolinite at $[Cd_{aq}]_{in}$ of 100 μM increased with increasing pH (Fig. 1a). The extent of Cd sorbed at pH values below ~7 could not be quantified; the extent of Cd(II) remaining in solution after the experimental sorption period was not significantly different from the control solutions. At pH values 7, 8, and 9, and under ambient conditions, approximately 3, 9 and 38% of $[Cd_{aq}]_{in}$ was sorbed at equilibrium, respectively, resulting in sorption densities of approximately 0.14, 0.32 and 1.43 μmol/m^2 (Table 1). Sorption of Cd under ambient and N^2 conditions showed the same trends (Fig. 1), suggesting that the presence of CO_2 and the potential precipitation of otavite did not contribute to loss of Cd(II) from solution in these experiments (i.e., there was no observed otavite formation). Further, loss of Cd in the control samples under ambient conditions over the 4 hour experimental period was less than 5%.

Analytical error of Cd(II) analysis by ICP–OES was 0.57% (1σ). The adsorption at pH 7, which is outer-sphere, may serve as a baseline for comparison for the other pH values, but with the caveat that the amount of outer-sphere adsorption may change with pH as the overall particle surface charge changes. The adsorption density at pH 7 under the experimental conditions (100 μM $[Cd_{aq}]_{in}$ and 0.1 M $NaClO_4$) was found to be ~0.14 μmol/m^2 (Table 1, Fig. 1a). Based on this value, outer-sphere sorption is predicted to account for approximately 50% of Cd(II) sorption at pH 8 and to contribute to a limited extent (<10%) to sorption at pH 9.

EXAFS analysis was performed on samples at pH 7, 8, and 9 from both ambient and N_2 experiments. EXAFS results for both conditions were consistent within fit uncertainties, and thus, discussion here is focused on the ambient samples. Precipitation of Cd-bearing solid phases was ruled out due to the absence of Cd–Cd coordination. Brief further discussion of precipitation

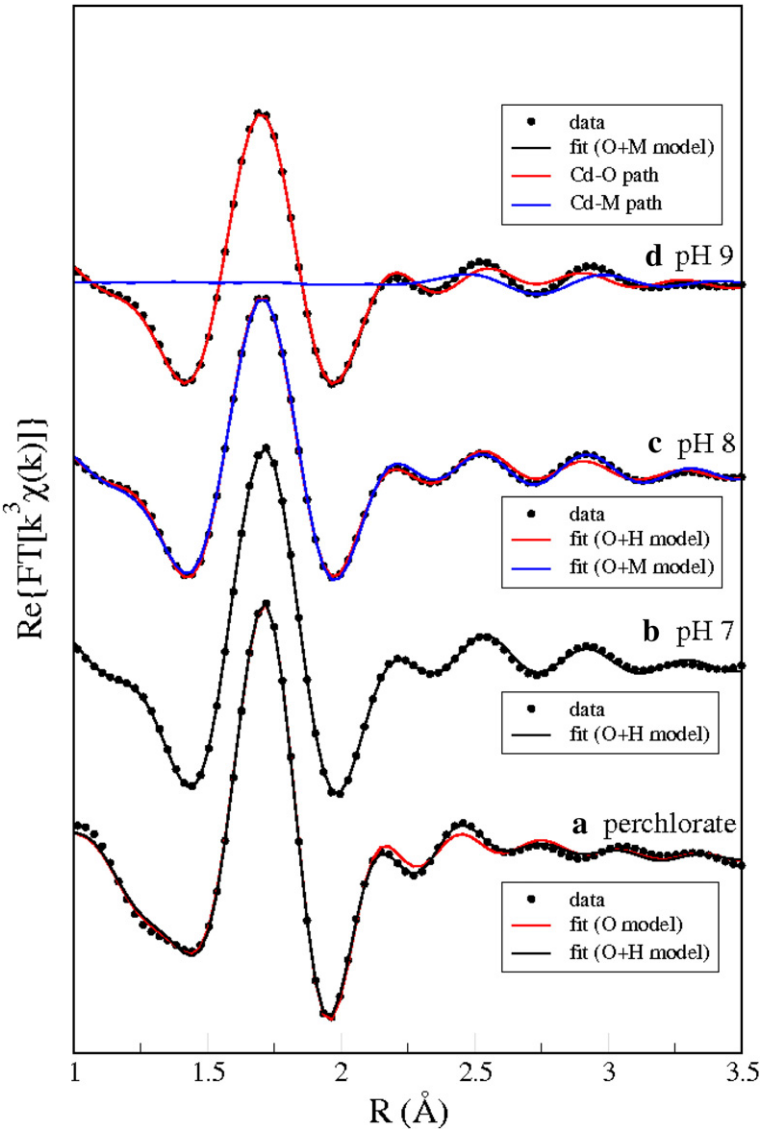

Fig. 3. (Color online) Fits for Cd perchlorate and pH series samples.

and samples prepared under N_2 conditions follows (section 3.3). EXAFS oscillations (multiplied by k^3 to enhance features at high k values) for ambient samples at pH 7, 8, and 9 and $[Cd_{aq}]_{in}$ of 100 μM, as well as the Cd(II) perchlorate standard, representing the hydrated Cd(II) cation, are shown in Fig. 2.

Fits to the adsorption edge samples and to the hydrated Cd (II) standard data are shown in Fig. 3. In order to minimize the noise level in the Fourier transformed data, the very last half-oscillation in each data set was left out of the transform. The kaolinite data were Fourier transformed in the range $k=2.1$ Å^{-1} to $k=8.6$ Å^{-1} while the perchlorate data were Fourier transformed in the range $k=2.1$ Å^{-1} to $k=9.5$ Å^{-1}. Hydrated Cd(II) (i.e. $Cd(ClO_4)_2$ standard) was fit using a simple model consisting of a hydration shell of 6 water molecules at Cd–O interatomic distance of 2.27 Å (Table 2), in agreement with the literature (Boyanov et al., 2003; Ohtaki and Radnai, 1993).

When sorbed as either an outer-sphere or inner-sphere complex, Cd(II), by definition will be surrounded most closely by oxygen atoms from waters of hydration (outer-sphere) or a combination of waters of hydration and oxygens from the clay surface that bind to the central metal atom and displace one or more waters of hydration. However, unlike metal cations like Pb, where anisotropy created by the lone pair induces different Pb–O distances for water oxygens and mineral oxygens (Bargar et al., 1997; Strawn and Sparks, 1999), oxygen distances surrounding Cd(II) (first shell range: $R=1.2$ Å to $R=2.2$ Å) have been successfully fit (low values of χ^2_ν and $\mathcal{R}$) using a single Cd–O shell (Boyanov et al., 2003). Excluding the Cd–O path contribution to the goodness-of-fit parameters (as discussed in sec. 2.3 above), the fit to the perchlorate data that includes a hydrogen path (Boyanov et al., 2003) yielded $\chi^2_\nu=698$ and $\mathcal{R}=0.021$ as opposed to $\chi^2_\nu=1710$ and $\mathcal{R}=0.083$ for the model with an oxygen path only.

Correspondingly, the sample at pH 7 was successfully fitted with a single layer of hydration, like that for the reference hydrated Cd(II). Again, as for the reference compound, including both an oxygen first shell and hydrogen second shell gave the best fit (Fig. 3b, Table 2). Because the EXAFS measurement was performed on pastes, the signal is heavily weighted toward adsorbed Cd(II) and not aqueous Cd(II). This result suggests that the Cd(II) cation is sorbed as an outer-sphere complex at pH 7, and that the layer of hydration surrounding the central Cd(II) ion is not disturbed by interactions with the surface, in a manner similar to what has been proposed by the molecular modeling studies of Vasconcelos et al. (2007). A schematic representation of the basal plane adsorption site is shown in Fig. 4a.

In contrast, this hydration model gives a poor fit to the sample at pH 9 (data not shown; $\chi^2_\nu=5026$ and $\mathcal{R}=0.110$). A good fit is achieved with a first shell of 4.9 oxygen atoms (Table 2) and without contribution from the hydrogen path. Inclusion of the Cd–O path alone was not sufficient to fit the feature in the EXAFS signal for this sample between $R=2.2$ Å and $R=3.2$ Å, as is clearly shown in Fig. 3d. A second shell arising from inner-sphere adsorption of Cd(II) at the kaolinite edge sites was thus included in the fit. At pH 9, previous studies have indicated that sorption is not dependent on ionic strength and is consistent with inner-sphere sorption at deprotonated edge sites. This second shell is given the label M to represent either Al or Si as they are not readily distinguishable by EXAFS, due to their similar backscattering amplitudes. Consistent with this, numerical values obtained from fits attempted using a O+Si model and a O+Al model were consistent within the uncertainties of the fit. Contribution from hydrogen atoms was not required to fit the sample at pH 9, which is also suggestive of inner-sphere sorption of Cd(II) to kaolinite at pH 9. Hydrogen atoms are not

Table 2
Fit results for Cd perchlorate and the pH series of samples

Shell	N	σ^2 (10^{-3} Å^{-2})	R (Å)	ΔE_0 (eV)	χ^2_ν	$\mathcal{R}$
(a) Cd(II) perchlorate						
O	6.0±0.2	8.7±0.5	2.27±0.01	−1.06±0.29	698	0.021
H	$2\times N_O$	17.6±7.2	2.93±0.04			
(b) Cd(II)+kaolinite−$[Cd_{aq}]_{in}$ 100 μM−pH 7						
O	5.9±0.2	9.0±0.9	2.27±0.01	−1.96±0.38	603	0.015
H	$2\times N_O$	10.5±6.2	2.91±0.04			
(c) Cd(II)+kaolinite−$[Cd_{aq}]_{in}$ 100 μM−pH 8						
Model 1						
O	4.8±0.3	9.0±1.4	2.26±0.01	−2.40±0.67	3582	0.055
H	$2\times N_O$	13.5±13.0	2.90±0.07			
Model 2						
O	5.1±0.3	10.1±1.3	2.27±0.01	−1.74±0.53	3500	0.053
M[a]	1 (fixed)	15.8±12.5	3.32±0.08			
(d) Cd(II)+kaolinite−$[Cd_{aq}]_{in}$ 100 μM−pH 9						
O	4.9±0.3	10.1±1.0	2.26±0.01	−2.14±0.54	1614	0.038
M[a]	1 (fixed)	12.3±5.8	3.34±0.04			

χ^2_ν and $\mathcal{R}$ restricted to the range $R=2.2$ Å to $R=3.2$ Å.
[a] Stands for either Al or Si (see text).

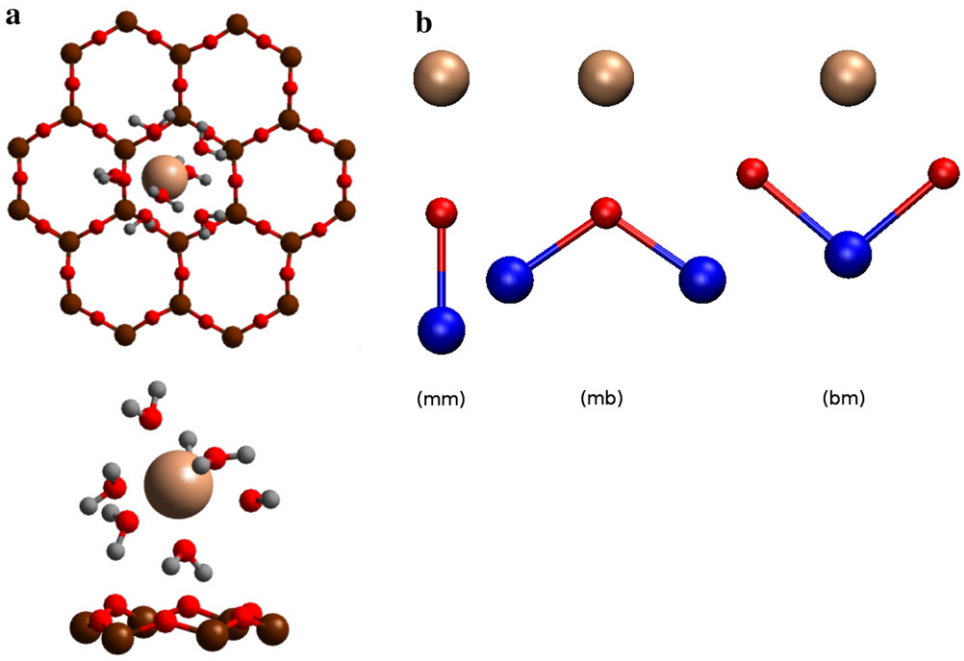

Fig. 4. (Color online) Schematic representation of possible adsorption sites on the surface of kaolinite. (a) basal plane site (from Vasconcelos et al. (2007)); (b) some edge site geometries: (mm) monodentate mononuclear; (mb) monodentate binuclear; (bm) bidentate mononuclear. Colors: Cd (brown), Al (blue), Si (maroon), O (red), and H (gray).

expected to contribute to the XAFS signal when there is disorder in the hydration shell (deviation from perfect octahedral symmetry) and/or in the presence of heavy backscatterers.

Fitting of the sample at pH 8 was not as straightforward as shown in Table 2 and Fig. 3c; neither the O+H nor the O+M models gave satisfactory results. A combination of the two models perhaps would give the best fit, and this is consistent with the fact that the pH value of this sample is intermediate to the samples at pH 7 (O+H model) and pH 9 (O+M model), so that perhaps more than one species or process occurs. However, the finite data range limits the resolution of Fourier transforms and prevents reliable separation of individual components of the two models in analysis of this sample.

3.2. Cd adsorption isotherm

The adsorption isotherm for Cd to kaolinite at pH 9 showed typical L-type sorption behavior (Sposito, 1984) with adsorption being outside of the linear range (i.e. approaching site saturation) at $[Cd_{aq}]_{in}$ of 100 μM (Fig. 1b). The O+M model that provided a good fit for the Cd–kaolinite samples at $[Cd_{aq}]_{in}$ of 100 μM was now applied to samples prepared at lower $[Cd_{aq}]_{in}$. Fig. 2 shows k^3-weighted $\chi(k)$ for the concentration series (3 μM, 10 μM, and 100 μM at pH 9). The amount of Cd adsorbed at $[Cd_{aq}]_{in}$ 10 μM and 3 μM is quite low (Table 1, Fig. 1) resulting in signal-to-noise ratios too small for EXAFS analysis. This problem was circumvented by inserting a 4-absorption-length Pd filter between the sample and the fluorescence detector, effectively filtering out the background and improving the signal-to-noise ratio to acceptable levels for quantitative analysis.

The three data sets were fit simultaneously with a single ΔE_0. This is a useful technique when applying the same model to fit a series of samples in which a few parameters change while the remaining are expected to be similar. Moreover, fitting data sets simultaneously increases the number of independent data points. This decreases errors associated with the fitting parameters and

Table 3
Fits to data for the concentration series of samples

Shell	N	σ^2 (10^{-3} Å^{-2})	R (Å)
(d) Cd(II)+kaolinite−[Cd_{aq}]$_{in}$ 100 μM−pH 9			
O	4.9±0.2	10.1±1.0	2.26±0.01
M	0.5	3.9±2.3	3.33±0.02
M	1.0	12.1±3.2	3.34±0.02
M	2.0	23.5±5.3	3.34±0.03
(g) Cd(II)+kaolinite−[Cd_{aq}]$_{in}$ 10 μM−pH 9			
O	5.1±0.3	11.0±1.1	2.26±0.01
M	0.5	4.9±4.9	3.26±0.03
M	1.0	13.6±6.9	3.27±0.04
M	2.0	25.7±9.9	3.27±0.06
(h) Cd(II)+kaolinite−[Cd_{aq}]$_{in}$ 3 μM−pH 9			
O	4.6±0.2	10.0±1.1	2.26±0.01
M	0.5	6.2±5.1	3.21±0.03
M	1.0	15.7±6.5	3.21±0.04
M	2.0	29.8±9.8	3.20±0.06

The first shell (O) parameters that yield the best fit were used to fit the second shell (M) for various fixed values of N_M. The three data sets were fitted simultaneously with a single ΔE_0 value and χ_ν^2 and $\mathcal{R}$ are restricted to the range R=2.2 Å to R=3.2 Å.
The following values were found:
N_M=0.5: ΔE_0=−2.38±0.45 eV, χ_ν^2=575, and $\mathcal{R}$=0.029.
N_M=1.0: ΔE_0=−2.17±0.23 eV, χ_ν^2=719, and $\mathcal{R}$=0.033.
N_M=2.0: ΔE_0=−2.01±0.52 eV, χ_ν^2=1483, and $\mathcal{R}$=0.067.

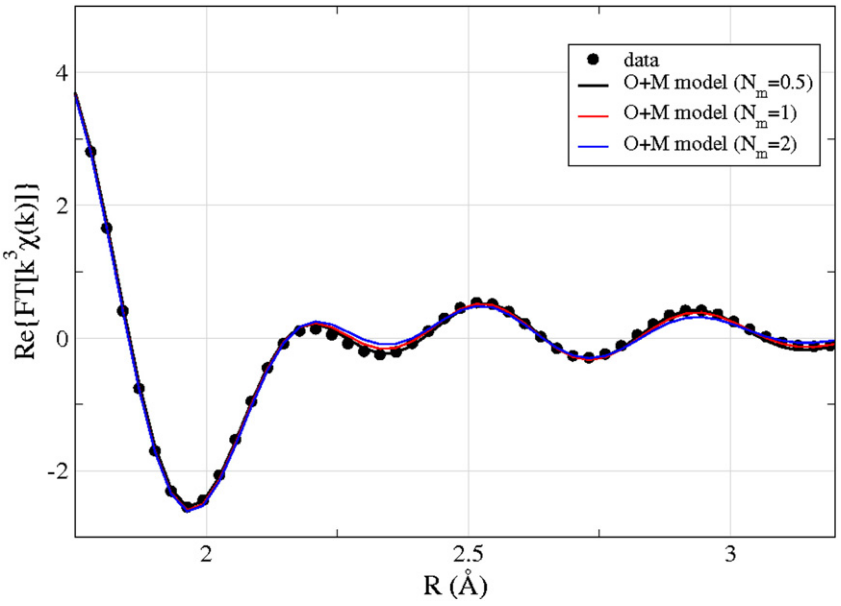

Fig. 5. (Color online) Fits to the data for the 100 μM and pH 9 sample using the O+M model with different fixed values of N_M.

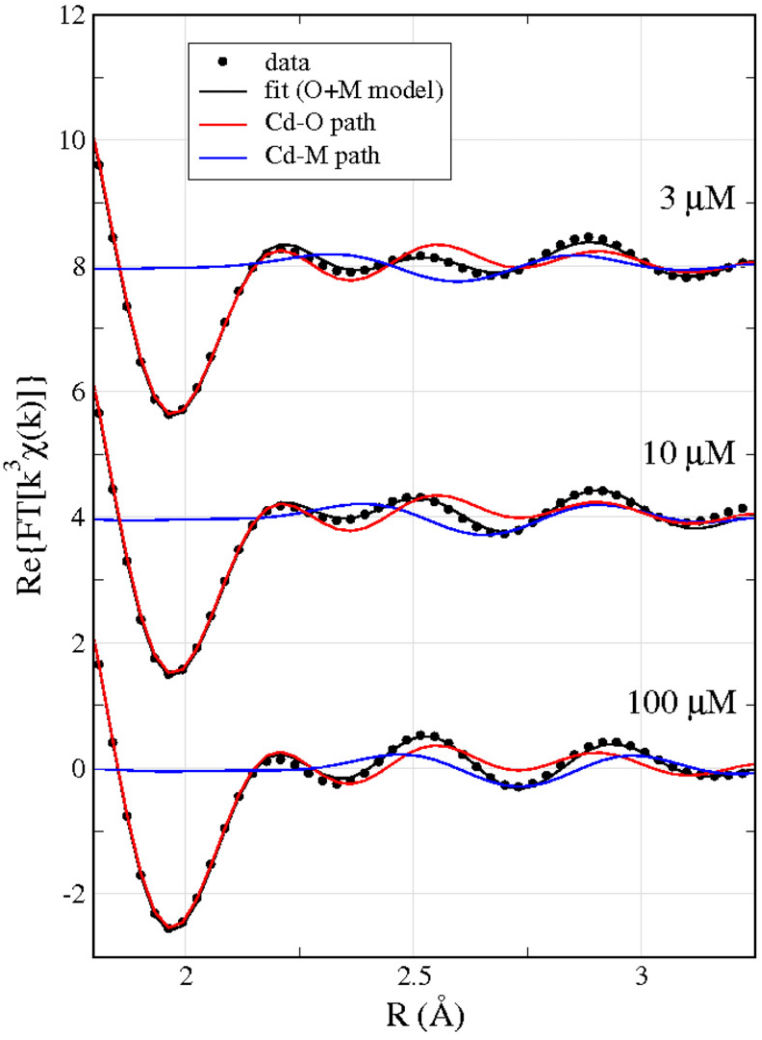

Fig. 6. (Color online) Fits to the data for the concentration series of samples. N_M value fixed at 1.

decreases correlations between variables, which ultimately results in increased confidence in the final fitted values. Simultaneous *k*-weightings of 1, 2, and 3 were also used in the fit. Like the adsorption edge series, absence of Cd–Cd coordination suggests precipitation of solid phases did not occur.

Because the contribution of the Cd–M path to the signal is very small, floating the three structural parameters (N, R, σ^2) results in an unstable fit with large error bars and unreliable results, whereas fixing one of the parameters to a certain value yields a robust, trustworthy fit. Fixing N in this case had the strongest physical basis. The coordination number of the bulk Cd(II) atom at the solid surface is expected to be at the most 2 (bidentante complex). The presence of amounts of Cd forming monodentate complexes and in a fully hydrated state should decrease this number but not by a large fraction.

Based on the arguments above, we fitted the second shell with fixed N_M of 0.5, 1, and 2 and let R and σ vary - the structural parameters relative to the Cd–O path that yield the best fit were used. We also tried a model with N_M=0.3 but rejected this possibility due to poor fit and unrealistic Debye–Waller factor values. The fit results are shown in Table 3. When the M coordination is fixed at 2, the model gives a comparably poor fit and yields very high Debye–Waller factors, clearly trying to minimize the M contribution. Values of χ^2_ν and $\mathcal{R}$ indicate that the best value of N_M lies between 0.5 and 1, which can be regarded as an indication of multiple sites involved. This can be visually inspected in Fig. 5. The Debye–Waller factors increase with rising N_M to compensate for the increase in amplitude. It is important to notice that the Cd–M distances obtained from the fits are virtually unchanged for each $[Cd_{maq}]_{in}$ regardless of the N_M value used.

Fig. 6 shows fits to the three data sets (with N_M=1) showing individual contributions of the Cd–O and Cd–M paths. As anticipated, the first shell of oxygen atoms does not change with changing $[Cd_{aq}]_{in}$. However, the distance shift in the Cd–M paths is very clear amongst samples, and this shift translates to an increase in the Cd–M distance with increased $[Cd_{aq}]_{in}$. Specifically, the Cd–M distance increased from 3.210 Å at 3 μM to 3.340 Å at 100 μM $[Cd_{aq}]_{in}$. These changes in interatomic distance are well outside the uncertainties and can thus be statistically considered real.

While the basal surface of kaolinite presents a preferred adsorption site at the hexagonal cavities, at the particle edges various possible adsorption geometries exist, be it an Al based or a Si based site. Moreover, researchers are not in complete agreement about the active participation of many of these sites and to what degree. It is important to point out that each geometry will yield a different Cd–M distance. To illustrate this point, three different Al–O^- inner-sphere Cd(II) adsorption geometries are shown in Fig. 4b. They are: monodentate-mononuclear (mm), monodentate-binuclear (mb), bidentate-monoclear (bm). The Cd–Al distances can be estimated as described below.

Assuming an Al–O distance of 1.93 Å (Bish, 1993) and a Cd–O distance of 2.26 Å (this work), the monodentate-mononuclear (mm) geometry suggests a Cd–Al distance of 4.22 Å, while the monodentate-binuclear (mb) geometry, assuming an Al–O–Al angle of 105° (Bish, 1993) suggests a Cd–Al distance of 3.75 Å. Finally, in the bidentate-mononuclear (bm) geometry there is no reason to believe the O–Al–O angle should be constrained as the Al–O bonds are free to dangle. In fact, Eng et al. (2000) point out that adsorption of aqueous complex to α-Al_2O_3 leads to significant surface relaxation. We assume that Cd would keep the octahedral arrangement of oxygen ions around it which imposes a O–Cd–O angle of about 90° (that is not totally true as the Cd–O coordination is found to be about 5 for the pH 9 samples (Table 3), which would indicate a slightly larger angle). The range of

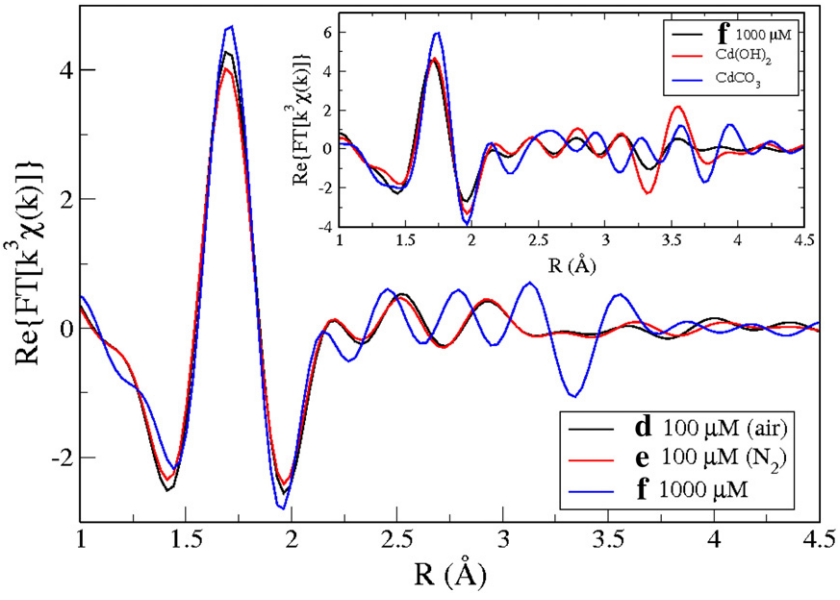

Fig. 7. (Color online) Real part of Fourier transform of the data for the precipitation study. The inset shows a comparison between the data for the 1000 μM samples and $Cd(OH)_2$ and $CdCO_3$ solid standards.

Table 4
Fit results for the precipitation study

Shell	N	σ^2 (10^{-3} Å^{-2})	R (Å)	ΔE_0 (eV)
(d) Cd(II) + kaolinite − [Cd_{aq}]$_{in}$ 100 μM − pH 9 (air)				
O	4.9±0.3	10.1±1.0	2.26±0.01	−2.14±0.54
M	1 (fixed)	12.3±5.8	3.34±0.04	
(e) Cd(II) + kaolinite − [Cd_{aq}]$_{in}$ 100 μM − pH 9 (N_2)				
O	4.6±0.3	10.3±1.1	2.26±0.01	−2.32±0.49
M	1 (fixed)	11.8±5.5	3.33±0.03	
(f) Cd(II) + kaolinite − [Cd_{aq}]$_{in}$ 1000 μM − pH 9				
O	6.2±0.6	9.6±1.7	2.29±0.01	1.69±0.39
O	1 (fixed)	5.8±2.0	2.55±0.01	
Cd	2.5±0.6	11.0±3.9	3.52±0.04	

Cd–M distances of 3.20–3.34 Å yields an Al–O–Al angle in the range 81° to 88°. For a non relaxed surface (Al–O–Al angle of 105°), the Cd–Al distance resulting is 2.68 Å.

The data presented here do not allow for reliable identification of which (if any) of these sites play a role in the adsorption process. The range of Cd–M distances found in this work is consistent with a combination of these sites. From the data set, it can be inferred that at certain pH ranges, a particular combination of inner-sphere Cd(II) complexes takes place. Further work is needed in order to check the validity of this inference.

3.3. Precipitation study

The control solutions (i.e., solutions in the absence of kaolinite) that were prepared under ambient conditions for adsorption edge experiments were theoretically supersaturated with respect to otavite. Yet, there was no evidence for otavite precipitation; there was no loss of Cd from control solutions. There was also not evidence from EXAFS of Cd–Cd interactions in kaolinite-containing samples. To ensure that we were correct in the conclusion that Cd-containing precipitates did not form in experimental solutions, either in the presence or absence of kaolinite, we conducted two additional experiments.

First, EXAFS signals were compared from samples at pH 9 and $[Cd_{aq}]_{in}$ of 100 μM between samples prepared under ambient and N_2 atmosphere (N_2 atmosphere would prevent Cd-carbonate in the form of otavite from forming). EXAFS oscillations (multiplied by k^3 to enhance features at high k values) are shown in Fig. 2. The O+M model was used to fit both samples. The EXAFS signals and fits to both samples

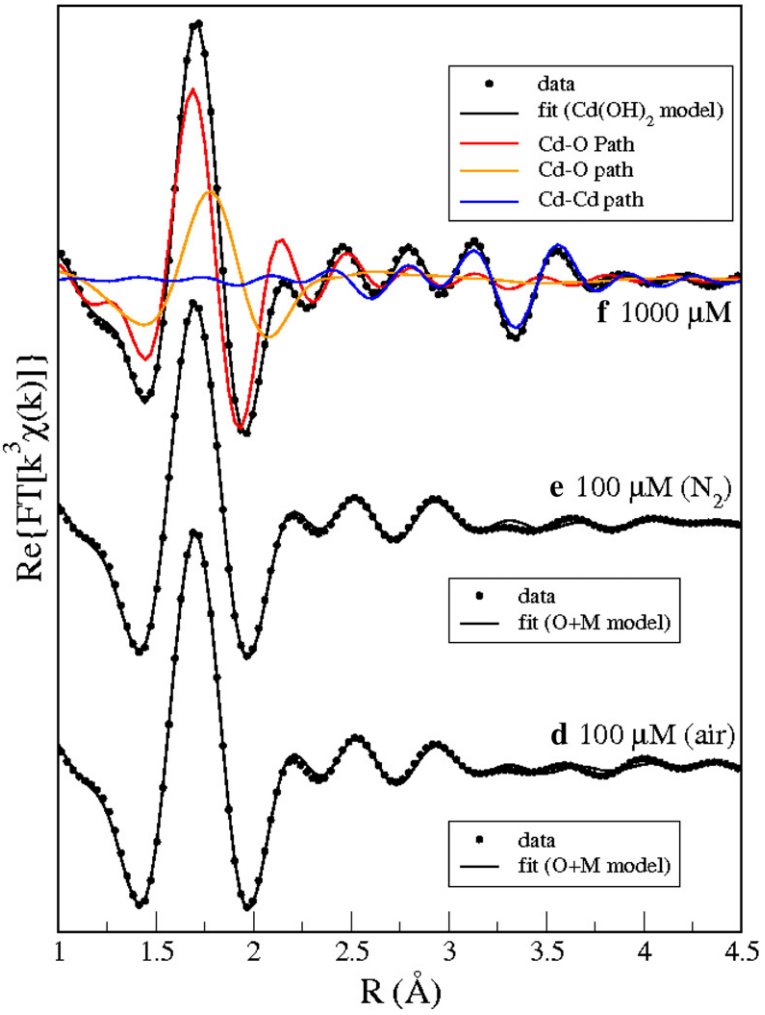

Fig. 8. (Color online) Fits to the data for the precipitation study.

show very similar structures and fitting parameters (Fig. 7 and Table 4). Neither sample shows spectroscopic evidence for the precipitation of otavite. Similar comparison was made at pH 8 and pH 7 with the same outcome (data not shown here).

Second, a Cd–kaolinite sample was prepared at the elevated $[Cd_{aq}]_{in}$ of 1000 μM and at pH 9 (Table 1) to promote precipitate formation. Once the pH was adjusted to 9, a white precipitate was immediately apparent. EXAFS analysis, including comparison with $CdCO_3$ and $Cd(OH)_2$ crystalline standards (Fig. 7, inset) suggested that the precipitate was $Cd(OH)_2$ rather than $CdCO_3$ (otavite). Comparison of EXAFS results from this experiment, including EXAFS of crystalline standards, with the Cd–kaolinite reacted samples confirmed the absence of Cd precipitates in the Cd–kaolinite experiments.

Quantitative confirmation of these assumptions are obtained from the fits to the data (Fig. 8). Fitting models based on the structure of $CdCO_3$ and $Cd(OH)_2$ were used in the attempts to fit the $[Cd_{aq}]_{in}$ 1000 μM data. As expected, the fit using the $CdCO_3$ model was unsatisfactory (not shown) while the Cd $(OH)_2$ model yielded a statistically good fit with fitting parameters consistent with the $Cd(OH)_2$ standard, as can be seen in Table 4. Thus, precipitation of otavite does not appear to occur even at elevated initial Cd concentrations under the conditions of our experiments. However, $Cd(OH)_2$ does form at high concentrations.

4. Summary and conclusions

The results of this work indicate pH dependence in the predominant mechanism(s) of Cd(II) uptake at the surface of kaolinite. At pH 7.0 and ionic strength of 0.1 M, the extent of Cd(II) adsorption is small and the local environment surrounding the adsorbed Cd(II) is not significantly different from that of hydrated Cd(II). These results are consistent with outer-sphere adsorption of Cd(II). This adsorption mechanism contrasts the mechanisms proposed by Schindler et al. (1987) based on batch uptake experiments of Cd to kaolinite. Those authors suggested that at pH 4–7 Cd(II) is adsorbed as an inner-sphere complex at AlOH edge sites. The proposed sites of Cd(II) adsorption at pH 7 is the kaolinite basal plane, based on the fact that previous work has shown Cd(II) adsorption to be essentially constant with pH at circumneutral values, and based on the XAFS results presented in this work. Adsorption of Cd(II) on the basal plane is corroborated by the molecular dynamics model of Vasconcelos et al. (2007), who showed that Cd(II) forms an outer-sphere complex with the kaolinite basal plane at pH 7, interacting only through electrostatic attraction.

With increased pH, there is increasing deprotonation of AlOH and SiOH sites on the edge of the kaolinite particles, although the Si sites deprotonate at low pH (Brady et al., 1996; Sutheimer et al., 1999). At pH 8, the extent of Cd adsorption had increased relative to that at pH 7, and the EXAFS results are most consistent with a more complex sorbed speciation of Cd (II) at this pH value; Cd(II) appears to be bound by a combination of both the inner-sphere complex that dominates sorption at pH 9 and the outer-sphere complex that dominates sorption at pH 7.

At pH 9, the extent of Cd(II) adsorption is increased and the EXAFS indicate that Cd(II) is adsorbed dominantly as an inner-sphere complex, although it is likely that some additional Cd(II) is still adsorbed outer-spherically on the basal plane. EXAFS analysis also confirmed that although predicted by thermodynamic modeling of the initial solution conditions (pre-adsorption), the precipitation of solid phases did not occur in amounts large enough to be identified by XAFS at $[Cd_{aq}]_{in}$ concentrations as high as 100 μM and following reaction time periods as long as 4 h.

At any concentration and pH where edge site adsorption dominates over siloxane basal surface adsorption, the EXAFS signal is expected to be a combination of contributions coming mostly from Cd adsorbed to Al-edge sites and also potentially some Si-edge sites. As pointed out above, Al and Si are similar backscatterers and therefore cannot be distinguished based just on their backscattering amplitude and phase. The most probable way to distinguish a Cd–Si site complex from a Cd–Al site complex would be if the Cd–Si and Cd–Al distances were further apart than the resolution of the Fourier transform.

For the $\chi(k)$ data range of 2.1 $Å^{-1}$ to 8.6 $Å^{-1}$ used in these studies, the resolution in R-space is approximately 0.25 Å, which by analysis of the numbers in Table 3, seems to be, in the best case scenario, comparable to the difference in distances. Our attempts to produce a model containing both Si and Al contributions failed to properly fit the data. Hence, although the EXAFS data indicate some change in the adsorption complexation as a function of loading at pH 9, we cannot distinguish whether this is due to a change in relative contributions of Si- versus Al- sites or to some other factor.

Thus, overall, our results indicate that Cd(II) may adsorb to kaolinite by a variety of different mechanisms as influenced by pH and $[Cd_{aq}]_{in}$. Further work expanding this research to different ionic strength and temperature conditions could help to better understand the potential array of controls on Cd sorption to kaolinite.

Acknowledgments

IFV thanks the Environmental and Molecular Science Institute (EMSI) at the University of Notre Dame for its support through the EMSI Graduate Student Scholarship. We wish to thank Drs. Randall Cygan and Bhoopesh Mishra for useful discussions. Beamtime setup help from the staff of MR-CAT is greatly appreciated. We thank the Natural Sciences and Engineering Research Council of Canada for support of EAH; the U.S. Department of Energy, Basic Energy Sciences, for funding this research; and the Center for Environmental Science and Technology and the Environmental Molecular Science Institute at the University of Notre Dame for use of facilities. Finally we would like to acknowledge the editor and the reviewers for the thorough and careful review.

References

Angove, M.J., Johnson, B.B., Wells, J.D., 1997. Adsorption of cadmium(II) on kaolinite. Colloids Surf., A 126, 137–147.

Ankudinov, A.L., Ravel, B., Rehr, J.J., 1998. Real-space multiple-scattering calculation and interpretation of X-ray absorption near-edge structure. Phys. Rev., B 58 (12), 7565–7576.

Bargar, J.R., Brown, G.E., Parks, G.A., 1997. Surface complexation of Pb(II) at oxide–water interfaces. 1. XAFS and bond-valence determination of mononu-22 clear and polynuclear Pb(II) sorption products on aluminum oxides. Geochim. Cosmochim. Acta 61, 2617–2637.

Bish, D.L., 1993. Rietveld refinement of the kaolinite structure at 1.5 K. Clays Clay Miner. 41, 738–744.

Boyanov, M.I., Kelly, S.D., Kemner, K.M., Bunker, B.A., Fein, J.B., Fowle, D.A., 2003. Adsorption of cadmium to *bacillus subtilis* bacterial cell walls: a pH-dependent X-ray absorption fine structure spectroscopy study. Geochim. Cosmochim. Acta 67, 3299–3311.

Brady, P.V., Cygan, R.T., Nagy, K.L., 1996. Molecular controls on kaolinite surface charge. J. Colloid Interface Sci. 183, 356–364.

Brown, G.E., Parks, G.A., 2001. Sorption of trace elements on mineral surfaces: modern perspectives from spectroscopic studies, and comments on sorption in the marine environment. Int. Geol. Rev. 43, 963–1073.

Brown, G.E., Calas, G., Hemley, R.J., 2006. Scientific advances made possible by user facilities. Elements 2, 23–30.

Chen, C.C., Hayes, K.F., 1999. X-ray absorption spectroscopy investigation of aqueous Co(II) and Sr(II) sorption at clay–water interfaces. Geochim. Cosmochim. Acta 63, 3205–3215.

Chorover, J., Sposito, G., 1995. Surface-charge characteristics of kaolinitic tropical soils. Geochim. Cosmochim. Acta 59, 875–884.

Eick, M.J., Naprstek, B.R., Brady, P.V., 2001. Kinetics of Ni(II) sorption and desorption on kaolinite: residence time effects. Soil Sci. 166, 11–17.

Eng, P.J., Trainor, T.P., Brown, G.E., Waychunas, G.A., Newville, M., Sutton, S.R., Rivers, M.L., 2000. Structure of the hydrated α-Al_2O_3(0001) surface. Science 288, 1029–1033.

EPA, 2002. Ground water & drinking water technical factsheet on: Cadmium. Environmental Protection Agency. Tech. rep.

Ferris, A.P., Jepson, W.B., 1975. Exchange capacities of kaolinite and preparation of homoionic clays. J Colloid Interface Sci 51, 245–259.

Hepinstall, S.E., Turner, B.F., Maurice, P.A., 2005. Effects of siderophores on Pb and Cd adsorption to kaolinite. Clay. Clay Miner. 53, 557–563.

Kaplan, D.I., Bertsch, P.M., Adriano, D.C., 1995. Facilitated transport of contaminant metals through an acidified aquifer. Ground Water 33, 708–718.

Kemner, K.M., Kropf, A.J., Bunker, B.A., 1994. A low-temperature total electron yield detector for X-ray absorption fine structure spectra. Rev. Sci. Instrum. 65, 3667–3669.

Koningsberger, D.C., Prins, R. (Eds.), 1988. X-ray absorption - principles, applications, techniques of EXAFS, SEXAFS and XANES. John Wiley & Sons, Inc.

Kugler, H., Ottner, F., Froeschl, H., Adamcova, R., Schwaighofer, B., 2002. Retention of inorganic pollutants in clayey base sealings of municipal landfills. Appl. Clay Sci. 21, 45–58.

Manceau, A., Marcus, M.A., Tamura, N., 2002. Quantitative speciation of heavy metals in soils and sediments by synchrotron X-ray techniques. Rev. Mineral. Geochem. 49, 341–428.

McNear, D.H., Tappero, R., Sparks, D.L., 2005. Shining light on metals in the environment. Elements 1, 211–216.

Newville, M., 2001. IFEFFIT: interactive EXAFS analysis and FEFF fitting. J. Synchrotron Radiat. 8, 322–324.

Newville, M., Livins, P., Yacoby, Y., Rehr, J.J., Stern, E.A., 1993. Near-edge X-ray-absorption fine-structure of Pb — a comparison of theory and experiment. Phys. Rev., B 47, 14126–14131.

O'Day, P.A., Parks, G.A., Brown, G.E., 1994. Molecular structure and binding sites of cobalt(II) surface complexes on kaolinite from X-ray absorption spectroscopy. Clays Clay Miner. 42, 337–355.

Ohtaki, H., Radnai, T., 1993. Structure and dynamics of hydrated ions. Chem. Rev. 93, 1157–1204.

Papelis, C., Brown, G.E., Parks, G.A., Leckie, J.O., 1995. X-ray absorption spectroscopy studies of cadmium and selenite adsorption on aluminum oxides. Langmuir 11, 2041–2048.

Papini, M.P., Majone, M., Rolle, E., 2001. Kaolinite sorption of Cd, Ni and Cu from landfill leachates: influence of leachate composition. Water Sci. Technol. 44, 343–350.

Parkhurst, D.L., Appelo, C.A.J., 1999. Users guide to PHREEQC (v. 2)-computer program for speciation, batch-reaction, one-dimensional transport, and inverse geochemical calculations. Tech. rep. USGS Water-Resources Investigations Report, pp. 99–4259.

Parkman, R.H., Charnock, J.M., Livens, F.R., Vaughan, D.J., 1998. A study of the interaction of strontium ions in aqueous solution with the surfaces of calcite and kaolinite. Geochim. Cosmochim. Acta 62, 1481–1492.

Peacock, C.L., Sherman, D.M., 2005. Surface complexation model for multisite adsorption of copper(II) onto kaolinite. Geochim Cosmochim Acta 69, 3733–3745.

Ravel, B., Newville, M., 2005. ATHENA, ARTEMIS, HEPHAESTUS: Data analysis for X-ray absorption spectroscopy using IFEFFIT. J. Synchrotron Radiat. 12, 537–541.

Sahai, N., Carroll, S.A., Roberts, S., O'Day, P.A., 2000. X-ray absorption spectroscopy of strontium(II) coordination. II. sorption and precipitation at kaolinite, amorphous silica, and goethite surfaces. J. Colloid Interface Sci. 222, 198–212.

Schindler, P.W., Liechti, P., Westall, J.C., 1987. Adsorption of copper, cadmium and lead from aqueous-solution to the kaolinite water interface. Neth. J. Agric. Sci. 35, 219–230.

Spark, K.M., Wells, J.D., Johnson, B.B., 1995. Characterizing trace metal adsorption on kaolinite. Eur. J. Soil Sci. 46, 633–640.

Sposito, G., 1984. The Surface Chemistry of Soils. Oxford University Press.

Sposito, G., 1990. Molecular-models of ion adsorption on mineral surfaces. Rev. Mineral. 23, 261–279.

Strawn, D.G., Sparks, D.L., 1999. The use of XAFS to distinguish between inner and outer-sphere lead adsorption complexes on montmorillonite. J. Colloid Interface Sci. 216, 257–269.

Sutheimer, S.H., Maurice, P.A., Zhou, Q.H., 1999. Dissolution of well and poorly crystallized kaolinites: Al speciation and effects of surface characteristics. Am. Mineral. 84, 620–628.

Thompson, H.A., Parks, G.A., Brown, G.E., 2000. Formation and release of cobalt(II) sorption and precipitation products in aging kaolinite–water slurries. J. Colloid Interface Sci. 222, 241–253.

Vasconcelos, I.F., Bunker, B.A., Cygan, R.T., 2007. Molecular dynamics modeling of ion adsorption to the basal surface of kaolinite. J. Phys. Chem. C 111, 6753–6762.

Yavuz, O., Altunkaynak, Y., Guzel, F., 2003. Removal of copper, nickel, cobalt and manganese from aqueous solution by kaolinite. Water Res. 37, 948–952.